

9. SIMULTANEOUS BOREHOLE AND OCEAN BOTTOM SEISMOMETER RECORDINGS OF EARTHQUAKES AND EXPLOSIONS: RESULTS FROM THE 1983 NGENDEI EXPERIMENT AT DEEP SEA DRILLING PROJECT HOLE 595B¹

P. M. Shearer, R. G. Adair, J. A. Orcutt, and T. H. Jordan, Scripps Institution of Oceanography²

ABSTRACT

We use data from the 1983 Ngendei Seismic Experiment in the southwest Pacific to compare vertical component seismograms recorded by a borehole seismometer with those from ocean bottom seismometers. The borehole seismometer, the Marine Seismic System (MSS), was emplaced 54 m into the oceanic crust at the Ngendei site. Ocean bottom seismometers (OBSs) from the Scripps Institution of Oceanography were located atop 70 m of sediment and all were within 0.5 km of the borehole. Numerous seismic refraction shots were recorded simultaneously by both the borehole and ocean bottom instruments, as well as a small number of regional earthquakes. The waveforms and instrument-corrected spectra for compressional waves from these events are nearly identical for the two different instruments, while the absolute amplitudes of the arrivals differ by no more than 4 dB. Since borehole noise levels are 10 to 15 dB lower than the seafloor levels, there is a general increase in the signal-to-noise ratio for the buried instrument. The similarity in absolute amplitudes for these observations agrees with results obtained from simple synthetic seismogram calculations.

INTRODUCTION

Ocean bottom seismometers, or OBSs, have been used for many years to record both earthquakes and seismic refraction shots. Ocean bottom records have substantial advantages over surface hydrophone data, including improved signal-to-noise ratios and three-component capability. However, they also suffer from "noise" caused by possible sediment reverberations and unknown effects of OBS-seafloor coupling. Borehole seismometers emplaced in oceanic basement are largely free from these problems and also offer the possibility of improved signal-to-noise ratios. Recently such borehole seismometers have been successfully deployed in Deep Sea Drilling Project (DSDP) drill holes (see e.g., Stephen, 1979, 1984, and Duennebieer et al., 1984), and Stephen (1979, 1984) has developed a number of innovative analysis techniques for use with subseafloor seismic data.

The 1983 Ngendei Experiment was designed to provide data from both OBS and borehole instruments. One of the experimental objectives was to simultaneously record earthquakes, seismic refraction shots, and background noise with both instrument types in order to compare their performance and response. The noise comparison results are detailed elsewhere in this volume (Adair et al., this volume) which also includes chapters describing the seismic refraction and teleseismic experiments. This chapter will compare the signals (earthquakes and explosions) recorded simultaneously by both ocean bottom and borehole seismometers and compare these results with those of the noise study.

EXPERIMENT DESCRIPTION

The Ngendei site is located at DSDP Hole 595B in the southwest Pacific, about 1500 km west-southwest of Tahiti (Fig. 1). This site was chosen partially because of its proximity to the Tonga Trench, which provided a source of earthquakes for the teleseismic experiment described elsewhere in this volume (Jordan et al., this volume). This is a very old part of the Pacific basin with an estimated age as great as 140 Ma (H. W. Menard, personal communication, 1984). The sediment cover at the site is 70 m thick, relatively thin considering the age of the crust. The original spreading direction at the site cannot be determined from the available magnetic and bathymetric information, although upper mantle anisotropy favors a spreading direction of northeast (Shearer et al., this volume). A more detailed description of the site is available in the introductory chapter.

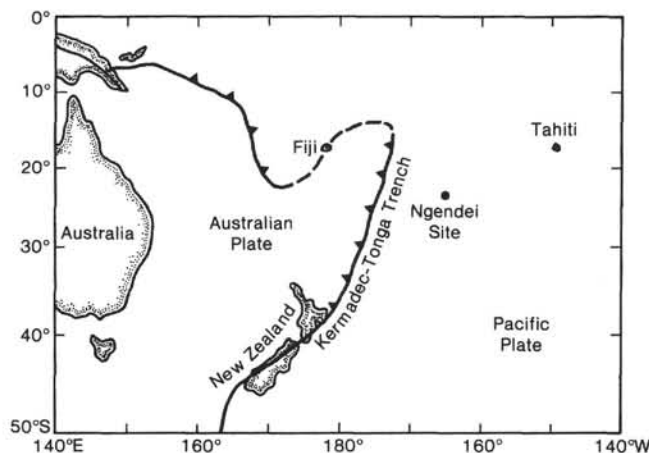


Figure 1. DSDP Hole 595B is located in the southwest Pacific about 1000 km east of the Tonga Trench.

¹ Menard, H. W., Natland, J., Jordan, T. H., Orcutt, J. A., et al., *Init. Repts. DSDP*, 91: Washington (U.S. Govt. Printing Office).

² Addresses: (Shearer, Adair, Orcutt) Institute of Geophysics and Planetary Physics, Scripps Institution of Oceanography (A-025), University of California, San Diego, La Jolla, CA 92093, (Adair, present address: Rockwell Hanford Operations, Energy Systems Group, P. O. Box 800, Richland, WA 99352); (Jordan, present address) Department of Earth, Atmospheric, and Planetary Sciences, Massachusetts Institute of Technology, Cambridge, MA 02139.

A borehole seismometer, the Marine Seismic System (MSS), was emplaced at the bottom of Hole 595B at a depth 124 m below the seafloor and 54 m into Layer 2. Data from a vertical and two horizontal seismometers were digitized at 40 samples/s and recorded on board the *Glomar Challenger*. An alternative recording system, the bottom processing package (BPP), also recorded some data after the departure of the *Challenger*. The frequency response of the MSS is shown in Figure 2. In this chapter, we will use data from the MSS short-period vertical seismometer recorded by both the Gould system (includes a finite impulse response, or FIR, anti-aliasing filter) and the Teledyne system (does not include FIR filter). The refraction shot data we will present were recorded by the Teledyne system; the earthquake and water wave data were recorded by the Gould system. Comparisons between Gould and Teledyne data have revealed that the Teledyne data are approximately a factor of 1.4 larger in amplitude than the Gould data, even after all appropriate gain adjustments have been made (Adair et al., this volume). Because the Teledyne data agreed with shipboard calibrations, we have taken the Teledyne amplitudes to be correct and have adjusted the Gould amplitudes upward by a factor of 1.4 for all analyses in this chapter.

OBSs from the Scripps Institution of Oceanography were deployed near the borehole for the seismic refraction experiment. Figure 3 shows approximate OBS locations relative to the borehole. Although other OBS deployments were made during the Ngendei experiment, in this chapter we will only examine data collected during the refraction deployments. The close proximity (0.5 km) of these OBSs to the borehole make this an ideal data set for comparisons of OBS and MSS data, since any effect of lateral variations between seismometer sites should be small. The OBSs are self-contained, digital instruments which record a vertical component, two horizontal components, and a hydrophone. Data are digitized

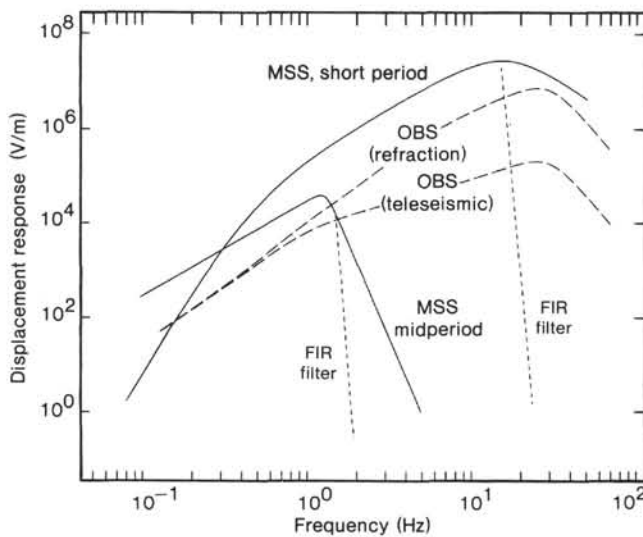


Figure 2. The frequency response of the instruments used in the Ngendei Experiment. This chapter discusses data from the MSS short-period seismometer and the OBS refraction configuration.

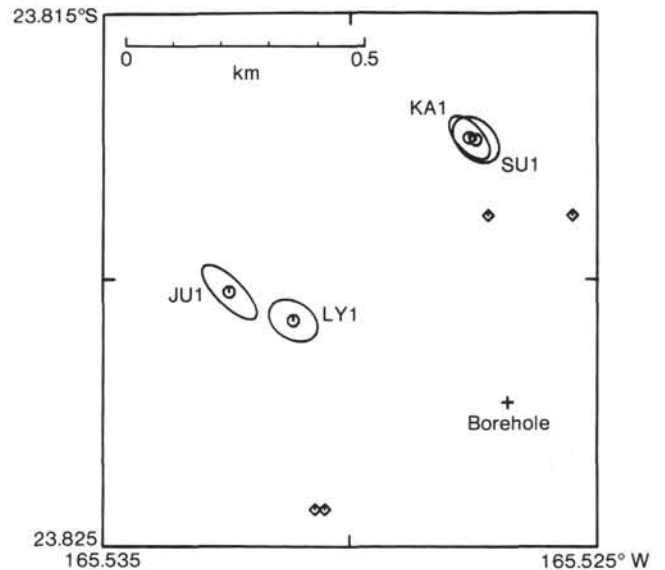


Figure 3. The Scripps Institution of Oceanography deployed four ocean bottom seismometers (OBSs) near the borehole for the seismic refraction experiment. This figure shows 95% confidence ellipses for the OBS locations relative to the borehole. Approximate drop points are shown as diamonds; OBS names are Karen, Suzy, Juan, and Lynn.

at 128 samples/s with approximately 13 s of data stored in memory before tape recorder activation. The memory size was increased for the teleseismic portion of the Ngendei experiment, but was limited to 13 s during the refraction deployments discussed in this chapter. The OBS frequency response during the refraction experiment is shown in Figure 2.

SEISMIC REFRACTION RECORDS

At least two OBSs recorded each of the lines shot during the refraction experiment. Unfortunately, delays in installing the borehole seismometer prevented its activation until the refraction shooting schedule was more than half completed. However, the MSS did record most of three refraction lines—Lines 4b, 5a, and 5b (see Fig. 5, Shearer et al., this volume or Shearer and Orcutt, 1985), which together contain over 250 shots recorded by both the MSS and two or more OBSs.

A comparison between an MSS record section and an OBS record section for Line 4b is presented in Figure 4. Both record sections have been corrected for topography, scaled by range and shot weight, and reduced at 8 km/s. The Moho triplication is prominent in both sections with the lower amplitude P_n arrival emerging at larger ranges. The broader frequency response of the OBS is apparent in these records as well as the improved signal-to-noise ratio of the MSS. Sediment reverberations and possible OBS-seafloor coupling oscillations show up in the OBS records as continued “ringing” following the initial P-wave and S-wave arrivals.

A comparison of MSS and OBS recordings in Figure 5 for P-wave arrivals from shots at ranges of 22, 40, and 58 km indicates coherence between the records is excellent for the first 1 to 2 s following the initial arrival and then begins to break down. Again one notices the greater

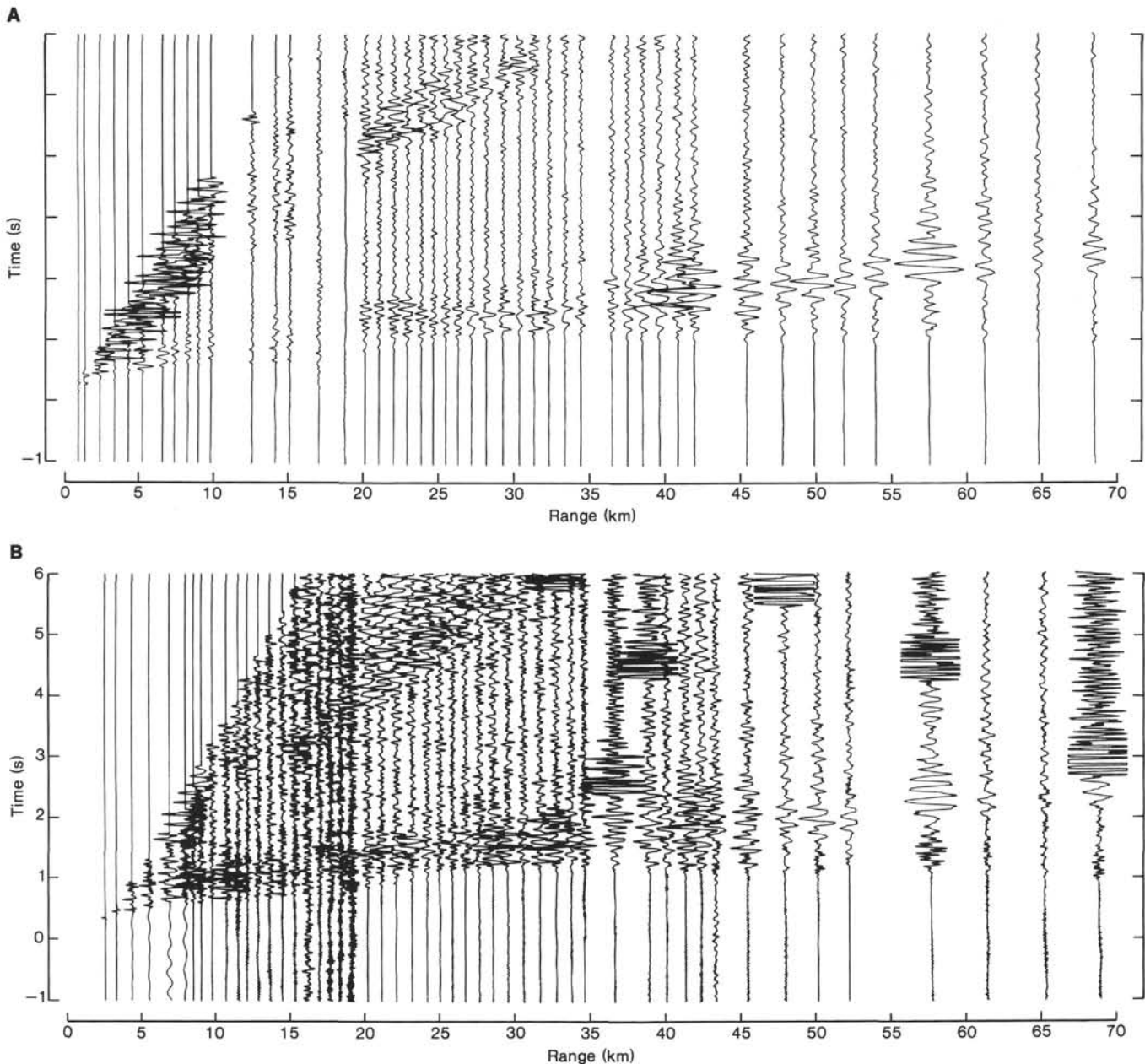


Figure 4. A comparison of vertical component seismic record sections of refraction Line 4b from (A) the MSS borehole seismometer and (B) OBS Karen. Times have been reduced at 8.0 km/s. Direct water wave arrivals, prominent in the MSS record, have been removed from the OBS record. The clipped, large amplitude phases in some of the OBS records at longer ranges are the result of tape recorder noise within the OBS capsule.

bandwidth of the OBS and the superior signal-to-noise ratio of the MSS. Shot 4269 (58 km range) shows both a P_n and a P_mP arrival. The higher frequency content of the P_n arrival relative to P_mP is apparent only in the OBS seismogram.

Figure 6 compares P-wave spectra between MSS and OBS for nine shots at ranges from 40 to 60 km. These were calculated by selecting 2.5-s windows following the initial P-wave arrival, applying a Hanning taper, calculating spectra, correcting for instrument response, and stacking the individual spectra to achieve a degree of stability. Agreement between the absolute amplitude and shape of the MSS and OBS spectra is remarkable. Average noise spectra for the MSS and OBS (also in Fig. 6)

were determined by stacking many separate simultaneous noise windows (Adair et al., this volume). Noise spectra vary somewhat between recording window times; we decided not to use windows immediately preceding the shot P waves because the records appear to be contaminated by reverberations from previous shots. Differences between noise spectra at different times are generally small for a given instrument, with lower frequency variations related to differences in weather conditions and higher frequency variations related to differences in ship noise. However, regardless of the particular shape of the noise spectra, OBS noise levels are consistently 10 to 15 dB higher than MSS noise levels. Figure 6 demonstrates that noise dominates the shot P-wave spectra at frequencies

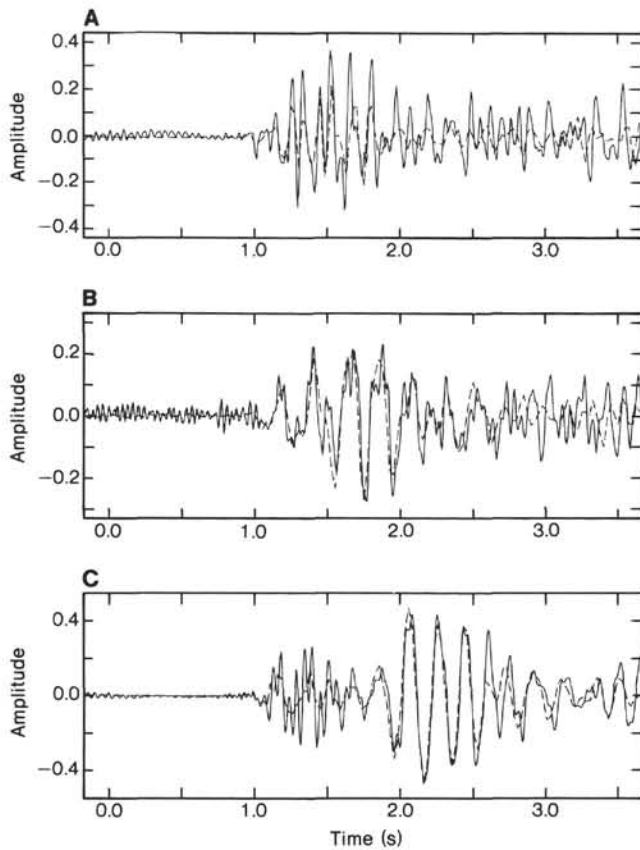


Figure 5. Comparison of vertical component MSS (dashed) and OBS (solid) recordings of P-wave arrivals from three Line 4b refraction shots. A. Shot 4242 (22 km). B. Shot 4260 (40 km). C. Shot 4269 (58 km). Shot 4269 shows both a P_n and P_mP phase. Note that the higher frequency content of the P_n arrival shows up only on the broader band OBS record.

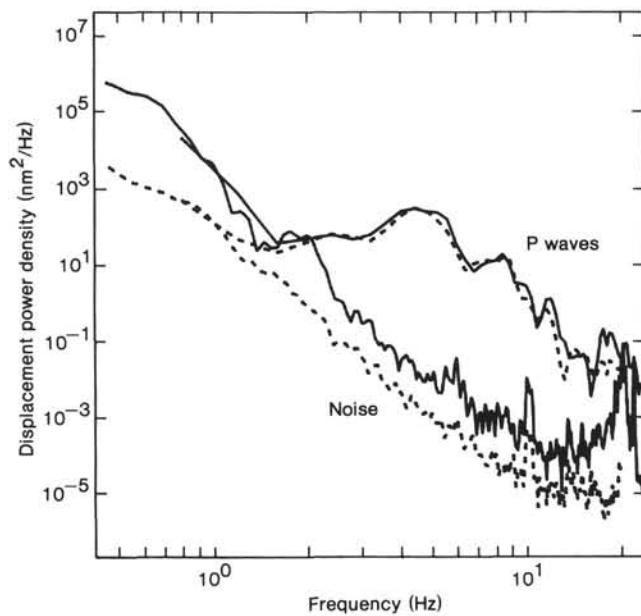


Figure 6. Comparison of vertical component MSS (dashed) and OBS Karen (solid) spectra of 2.5 seconds of P wave for nine shots from Line 4b at ranges of 40 to 60 km. Average noise spectra are shown below for comparison. The MSS enjoys a signal-to-noise advantage for recording these shots of 9 to 14 dB.

lower than about 2 Hz, a frequency well below the bubble pulse frequency of the shots. At higher frequencies, the nearly identical P-wave response coupled with the much lower MSS noise levels indicates a signal-to-noise improvement of about 9 to 14 dB for the MSS over the OBS.

Integrated total power between 3 and 20 Hz indicates that the OBS P-wave power is approximately a factor of 1.2 larger than the MSS P-wave power. We conducted a numerical experiment using a simple WKBJ synthetic algorithm to test this observation of near equality of the signals at the two depths. The model used was based on traveltimes and amplitude analyses of the Ngendei data (see Shearer et al., this volume) and physical properties measurements of the recovered sediments (see Kim et al., this volume). The sediments were taken to be 70 m thick and were characterized by a compressional-velocity gradient from 1.55 km/s at the seafloor to 1.65 km/s at the sediment/basement interface. In the same interval the shear-wave velocity increased from 100 m/s to 150 m/s. The basement velocity below the sediments was 4.6 km/s and increased rapidly with depth in the upper crust.

Synthetic seismograms for this model structure were calculated for both seafloor and intracrustal receivers between ranges of 40 and 60 km. For the seafloor receiver (OBS) the upgoing P ray (with accompanying P and SV reflections) was considered, while for the crustal receiver (MSS) the upgoing P ray as well as the compressional and shear waves reflected from the overlying sediment/basement interface were included. We found that the later reflections from the water/sediment interface were much smaller and could be neglected in these calculations. For a range of 45 km, which was fairly typical, the OBS synthetic amplitude was a factor of 2.16 smaller than the synthetic amplitude for the MSS receiver. This 6-dB difference contrasts somewhat with observations, but can be largely attributed to likely calibration uncertainties in the two instruments and the simplicity of the synthetic calculation. The calculation does confirm that the observed vertical amplitudes at the two levels should be comparable and that any reduction in noise level achieved by insertion in a borehole should lead to a direct increase in signal-to-noise levels.

EARTHQUAKE RECORDS

Following the refraction shooting, the MSS and six OBSs were left on the seafloor for 45 days to record earthquakes. The OBSs operated in trigger mode and recorded dozens of regional earthquakes and teleseisms during this time period. The MSS was connected to a BPP, which was designed to record continuously for 45 days. Unfortunately, the BPP failed after less than 2 days and captured only three earthquakes recorded by the OBSs during their 45-day deployment. Because of the failure of the BPP, the few days of shipboard recording of the MSS have proven invaluable. Many earthquakes were recorded during and immediately after the refraction shooting. During this time, 13 earthquakes were recorded by both the MSS and at least one OBS. Many of the OBS earthquake recordings were made by OBSs deployed for the refraction experiment, but which reverted to trigger mode following the end of shooting. In many cases, the

OBS earthquake records do not include the initial P-wave arrival since the OBS triggered on S or a later part of the P wave. Thus, there are a very limited number of recordings available for MSS versus OBS comparisons of the first arriving P wave.

Figure 7 compares MSS and OBS vertical component recordings of two regional earthquakes at an approximate 7-degree range. These events are not listed in the Preliminary Determination of Epicenters (National Earthquake Information Service, 1983) and we are aware of no other recordings of them. Each figure shows the MSS record of the entire seismogram, including both the P and S phases. Below this is an expanded view of the first 10 s of the P wave train as recorded by the MSS and an OBS. We do not show any more of the OBS record because it is contaminated by tape recorder noise from within the OBS capsule. As we saw in the refraction shot comparison, the broader frequency response of the OBS is apparent as well as the superior signal-to-noise ratio of the borehole instrument.

The MSS and OBS seismograms for the February 8, 1983 event are compared in detail in Figure 8. Coherence between the traces is excellent for the first few seconds and still fairly good even up to 8 s following the first arrival. The lessened coherence and higher OBS amplitudes in the latter part of this record probably resulted from superior OBS sensitivity to reverberations within the sediment layer and possible resonances in the OBS-seafloor system. At roughly 8 s following the initial P wave, a surface related phase (resulting from a bounce off the surface of the ocean) is much clearer on the OBS record than on the MSS record.

P-wave spectra for the two earthquakes are plotted in Figure 9. We windowed 10 s of the P wave with a Hanning taper, computed spectra, and corrected them for instrument response. These power spectra differ from others in this chapter in that stacking could not be employed to reduce the variance of the spectral estimates. The figures also show average noise spectra for the MSS versus the OBS. The signal-to-noise advantage of the MSS is apparent in these spectra but less pronounced than in the refraction shot comparison. This reduction of the signal-to-noise ratio arises because the OBS amplitudes for the earthquakes are somewhat higher than the MSS amplitudes. Integrated power from 3 to 20 Hz is about 2.3 times larger for the OBS (2.7 for Feb. 8 quake, 2.0 for Feb. 9 quake). The signal-to-noise advantage of the MSS for these earthquakes is about 6 to 11 dB. A possible cause for the higher earthquake OBS power levels relative to the refraction shots is the additional power in the sediment reverberations which were not included in the earlier analysis of refraction data.

DIRECT WATER WAVES

We also examined the direct water waves recorded during the refraction shooting in order to examine MSS and OBS differences in the decay of water arrivals with range. Figure 10 compares MSS and OBS Suzy vertical component record sections for Line 5b. Times have been reduced at 1.5 km/s in order to isolate the water wave arrivals. The direct water wave is the first arrival shown in

the sections, followed by the first water wave multiple, second multiple, etc. The OBS section is less complete because of the limited OBS recording window for each shot. In addition, most of the water waves are clipped on the OBS, and OBS tape recorder noise contaminates many of the water wave multiples.

In order to quickly examine the power level of a large number of water waves, we used a much simpler comparison method than the spectral comparisons discussed earlier in this chapter. We picked arrival times for the direct water wave for both the MSS and the OBS. Using a 1-s window following these picks we calculated an approximate power for each water wave arrival by computing the variance. Assuming a uniform 1.5 km/s ocean we also calculated the length of the diagonal ray path through the ocean appropriate for each shot. Figure 11 shows the power from the direct water wave versus water path length for both the MSS and the OBS. The MSS did not clip on any of the water wave arrivals, but only a few unclipped water waves are available for the OBS. Direct comparison of the MSS and OBS power levels measured in this way is, of course, not meaningful because of the differences in instrument responses. In order to obtain an approximate value for the difference in MSS and OBS water wave power, we calculated displacement power spectra for a 1-s window following the water wave arrival for shot 5030 (20-km range). After correcting for instrument responses, we integrated the power between 5 and 20 Hz and obtained a ratio of 3.5 for the OBS versus MSS water wave power, a value which we then used to constrain the relative positions of the MSS and OBS power curves in Figure 11.

The MSS amplitudes are smaller than the amplitudes measured on the OBS. This ratio of amplitudes is expected, given that the incident waves are largely reflected at the seafloor and the MSS must be excited, for the most part, by an evanescent wave which decays exponentially in amplitude in a vertical direction. The predicted amplitude ratio could not be computed with the simple WKB formalism; detailed comparisons were deferred for future investigations.

At water path lengths of 17 to 25 km (the range of the OBS data) the rate of falloff is approximately the same for the MSS and the OBS. A simple model of a uniform 1.5 km/s ocean predicts a r^{-4} falloff of power at the seafloor with path length. This results from an r^{-2} geometrical spreading term and an r^{-2} term to correct displacements along the ray path to vertical displacements. The OBS water wave power falls off slightly faster than r^{-4} . It is possible that this difference can be explained by tracing rays through a realistic ocean velocity profile. However, the steeper falloff shown in the MSS record at shorter ranges cannot be explained in this way and may reflect the evanescent behavior of the direct wave "root" (Stephen, 1984). That is, because the MSS is located 124 m below the seafloor (70 m of sediment, 54 m of rock), the direct water wave is critically reflected at the longer ranges and its amplitude below the seafloor cannot be predicted with simple geometrical ray theory. We plan further investigations of these data to see what, if anything, can be learned about the velocity

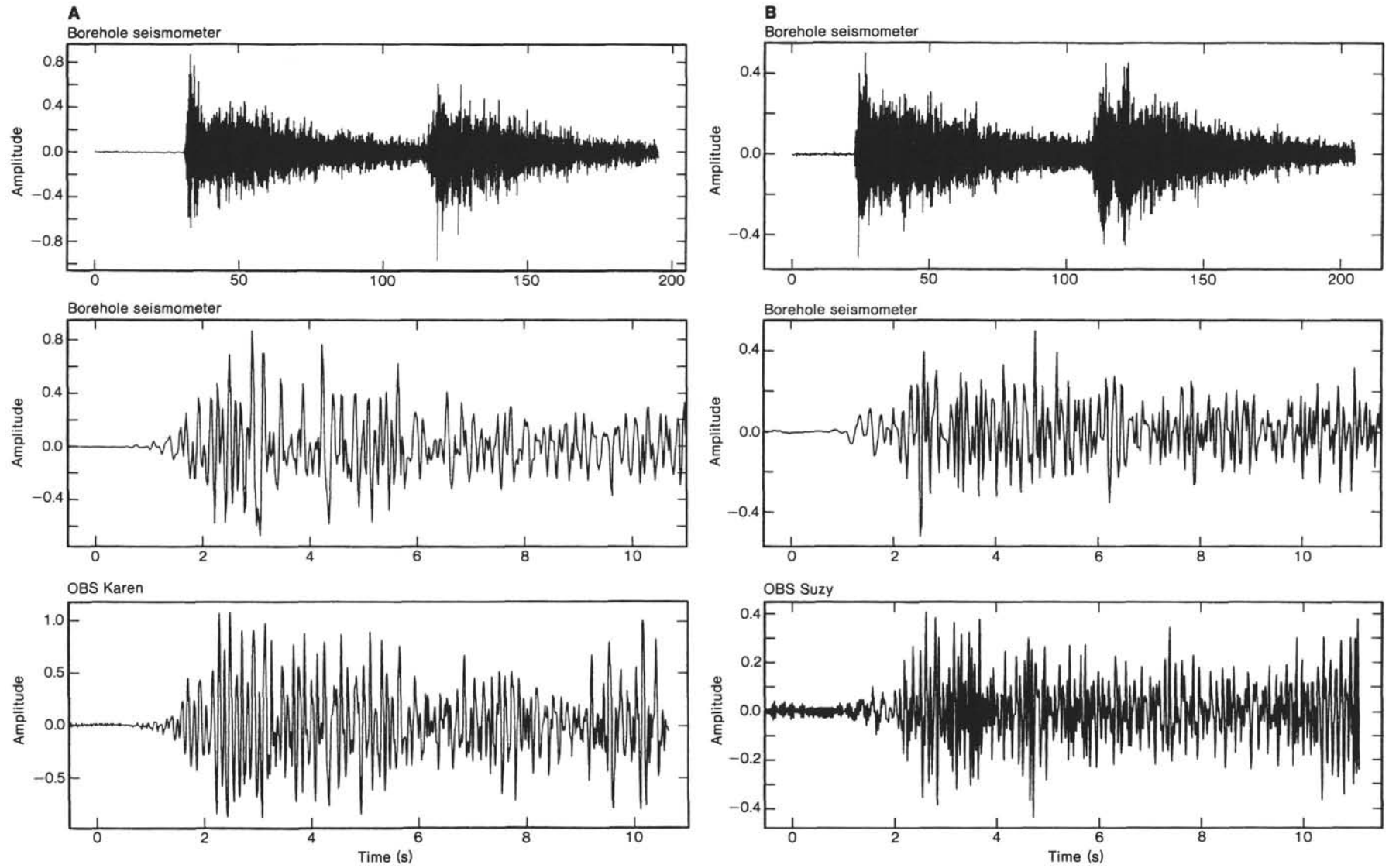


Figure 7. MSS and OBS vertical component recording of regional earthquakes. A. P-wave arrival at about 1036 UT, February 8, 1983. B. P-wave arrival at about 1433 UT, February 9, 1983. Top: MSS record of entire seismogram. Middle: first 10 s of P-wave train recorded by MSS. Bottom: first 10 s of P-wave train recorded by OBS.

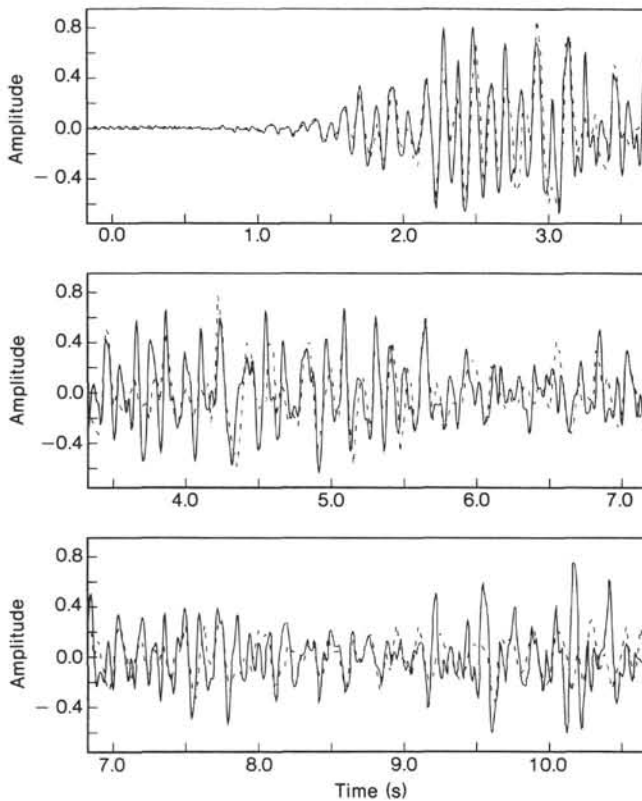


Figure 8. Comparison of vertical component MSS and OBS recording of the February 8 earthquake. MSS record is shown as a dashed line; OBS record is shown as a solid line.

of the sediment and shallow crust from water wave data of this type. One interesting feature of the data shown in Figure 11 is the peak in power at a path length of 8 km. This is likely related to the caustic associated with the emergence of the shear wave in the basement (Burnett et al., 1984; White, 1979).

CONCLUSIONS

Ocean bottom and borehole seismometer data exhibit excellent coherence for P wave recorded from both seismic refraction shots and regional earthquakes. The measured ratio of OBS power to MSS power is about 1.2 for explosions and 2.3 for regional earthquakes, values comparable to those predicted by theory. Since MSS noise levels are about 10 to 15 dB below OBS noise levels, this results in a signal-to-noise improvement of as much as 14 dB for the MSS over the OBS in recording explosions and 11 dB in recording earthquakes. These values are more certain than the measurements of absolute power level differences, since any instrument miscalibration presumably would have an equal effect on both the noise and signal amplitude measurements. Analysis of water wave arrivals shows that MSS direct water wave power levels fall off faster with range than would be predicted from a simple ray theory model.

REFERENCES

- Burnett, M. S., Orcutt, J. A., and McClain, J. S., 1984. Synthetic modeling of vertical component OBS water wave data. *EOS, Trans. Am. Geophys. Union*, 65:1013.
- Duennebie, F. K., Cessaro, R. K., Harris, D., and Anderson, P., 1984. The ocean sub-bottom seismometer: Results from the DSDP Leg 88 Borehole Seismic Experiment. *EOS, Trans. Am. Geophys. Union*, 65:1007.
- Shearer, P., and Orcutt, J., 1985. Anisotropy in the oceanic lithosphere—theory and observations from the Ngendei seismic refraction experiment in the southwest Pacific. *Geophys. J. R. Astron. Soc.*, 80:493–526.
- Stephen, R. A., 1979. The Oblique Seismic Experiment in oceanic crust—Experiment and technique. *Mar. Geophys. Res.*, 4:213–276.
- , 1984. The direct wave root in marine seismology. *EOS, Trans. Am. Geophys. Union*, 65:239.
- White, R. S., 1979. Oceanic upper crustal structure from variable angle seismic reflection-refraction profiles. *Geophys. J. R. Astron. Soc.*, 57:683–726.

Date of Initial Receipt: 22 March 1985

Date of Acceptance: 23 September 1985

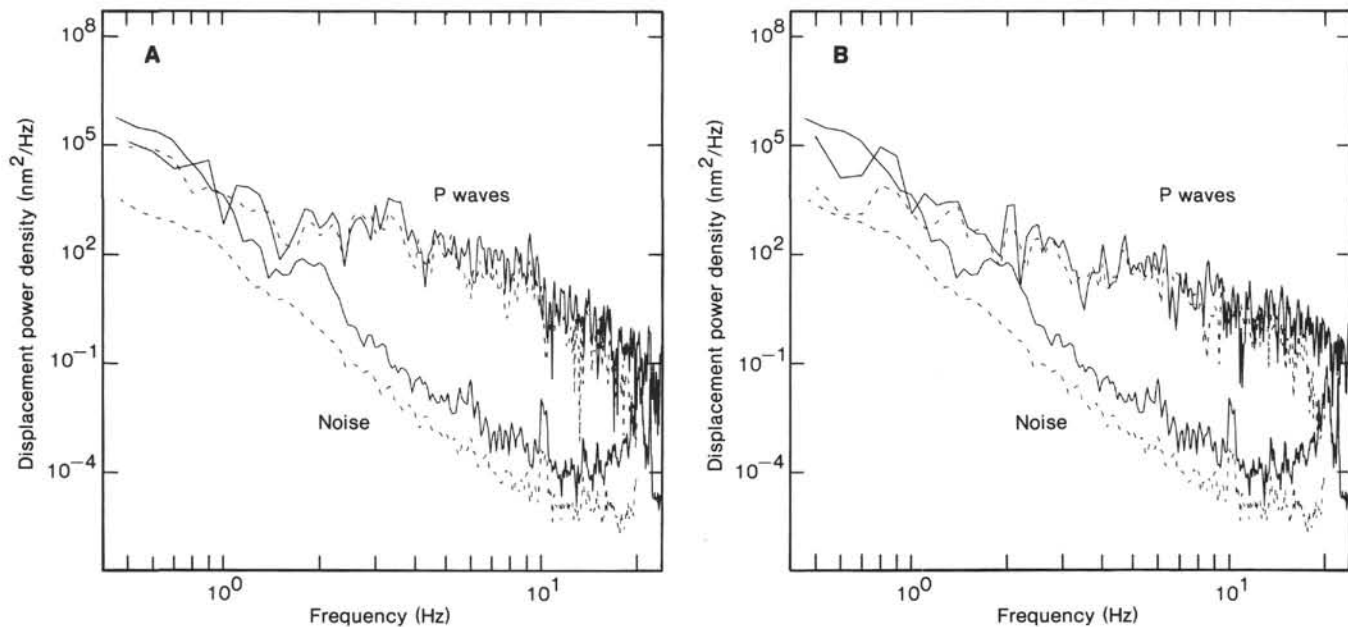


Figure 9. Comparison of vertical component MSS (dashed) and OBS (solid) spectra of 10 s of the initial P wave from (A) February 8, 1983 earthquake (OBS Karen) and (B) February 9, 1983 earthquake (OBS Suzy). Average noise spectra are shown for comparison.

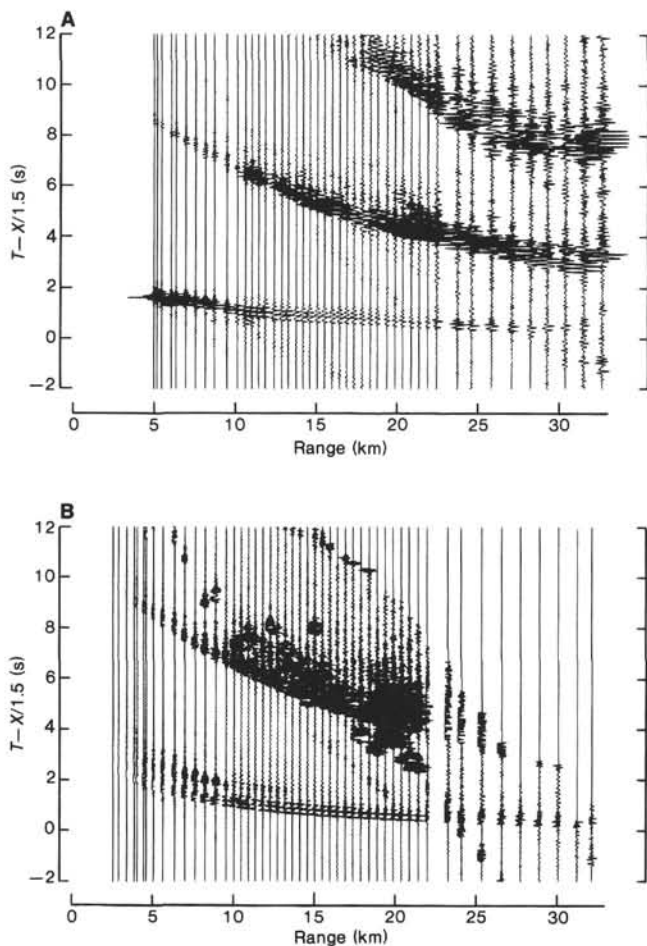


Figure 10. Line 5b water wave arrivals as recorded by (A) MSS and (B) OBS Suzy vertical seismometers. Record sections are reduced at 1.5 km/s in order to show the water waves and are scaled for range and shot weight.

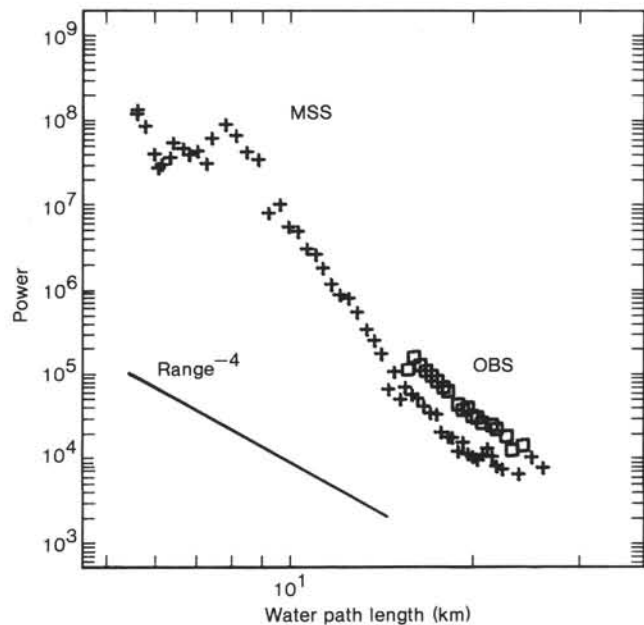


Figure 11. Comparison of direct water wave power (Line 5a) between the MSS and OBS Suzy for the vertical inertial components. Power has been scaled for shot weight by the factor $(w/w_0)^{1.3}$.